minerals

MDPI

Article

Genesis of Carbonate Breccia Containing Invisible Gold in Taebaeksan Basin, South Korea

Sang-Gun No [1], Maeng-Eon Park [2], Bong-Chul Yoo [3,4] and Seung-Han Lee [1,*]

[1] Mineral Resources Research Division, Korea Institute of Geoscience and Mineral Resources, Daejeon 34132, Korea; geologist@kigam.re.kr

[2] Department of Earth and Environmental Science, Pukyong National University, Busan 48513, Korea; mepark@pknu.ac.kr

[3] Convergence Research Center for Development of Mineral Resources, Korea Institute of Geoscience and Mineral Resources, Daejeon 34132, Korea; chbong@kigam.re.kr

[4] Department of Mineral and Groundwater Resources, University of Science and Technology, Daejeon 34113, Korea

* Correspondence: shlee91@kigam.re.kr; Tel.: +82-10-9140-3818

Received: 12 November 2020; Accepted: 2 December 2020; Published: 3 December 2020

Abstract: The Yemi breccia developed and is distributed within the Paleozoic carbonate rock (Maggol Formation) in the central part of the Taebaeksan Basin, South Korea. Explanation for the genesis of the Yemi breccia has been controversial. We investigated the petrological and mineralogical properties of the breccia and the matrix materials at 60 outcrops. The Yemi breccia is divided into crackle, mosaic, and chaotic breccias based on morphology. In addition, these are divided into blackish, reddish, grayish, and white to pinkish matrix breccias according to the materials of the matrix. Quartz, calcite, pyrite, hematite (after pyrite), and minor epidote, chlorite, and opaque materials mainly comprise the matrix materials. The pyrite grains from the Yemi breccia can be divided into two types based on the mineral texture: diagenetic and hydrothermal. We analyzed the chemistry of pyrite and hematite (after pyrite) from the Yemi breccia with an electron probe X-ray microanalyzer (EPMA). Invisible gold was detected within the pyrite grains by EPMA and disseminated micron-sized isolated gold particles were discovered by backscattered electron (BSE) images. The texture of Au-bearing pyrite and gold particles in the Yemi breccia is especially well matched with pyrite and gold from the Shuiyindong Carlin-type hydrothermal gold deposits, China. Therefore, we suggest an important role of hydrothermal fluid in karstification within the Paleozoic carbonate rock.

Keywords: Yemi breccia; matrix materials; pyrite; invisible gold; isolated gold particles; hydrothermal fluid; karstification

1. Introduction

The carbonate Yemi breccia developed in the Taebaeksan Basin in the northeastern part of the southern Korean Peninsula (Figure 1). It is distributed within an area that extends approximately 10 km north-to-south and 3 km east-to-west in the Yemi area (Figure 2). The genesis of the breccia has been reported variously as intraformational brecciation or intrusion of argillaceous materials in the cracks made by deformation; synsedimentation breccia related fault activities; syngenetic fault breccia during formation of a sediment basin; solution collapse breccia formed by dissolution of pre-existing evaporites; or diagenesis based on the occurrence of clasts, matrix mineralogy, fossils, and sedimentary structures [1–5]. On the other hand, it is reported that some breccias can be formed by the introduction of hydrothermal fluid along bedding or strata boundaries in carbonate rocks [6–14]. Breccias may have hydrothermal and hydraulic fracturing origin [15,16], formed by processes similar to typical karstification [6]. Their morphology is very similar to typical karst breccias formed by meteoric

water [17,18]. However, previous studies did not consider the theory that brecciation originated by hydrothermal fluid. Previous studies have reported the genesis of this breccia, but it is still controversial. Here we investigated the morphology and mineralogy of the infilled matrix of the breccia to clarify the genesis. In particular, we discovered invisible gold in pyrite and isolated gold particles in the Yemi breccia. As a result, we suggest that hydrothermal fluid acted in the development of the Yemi breccia within carbonate rock.

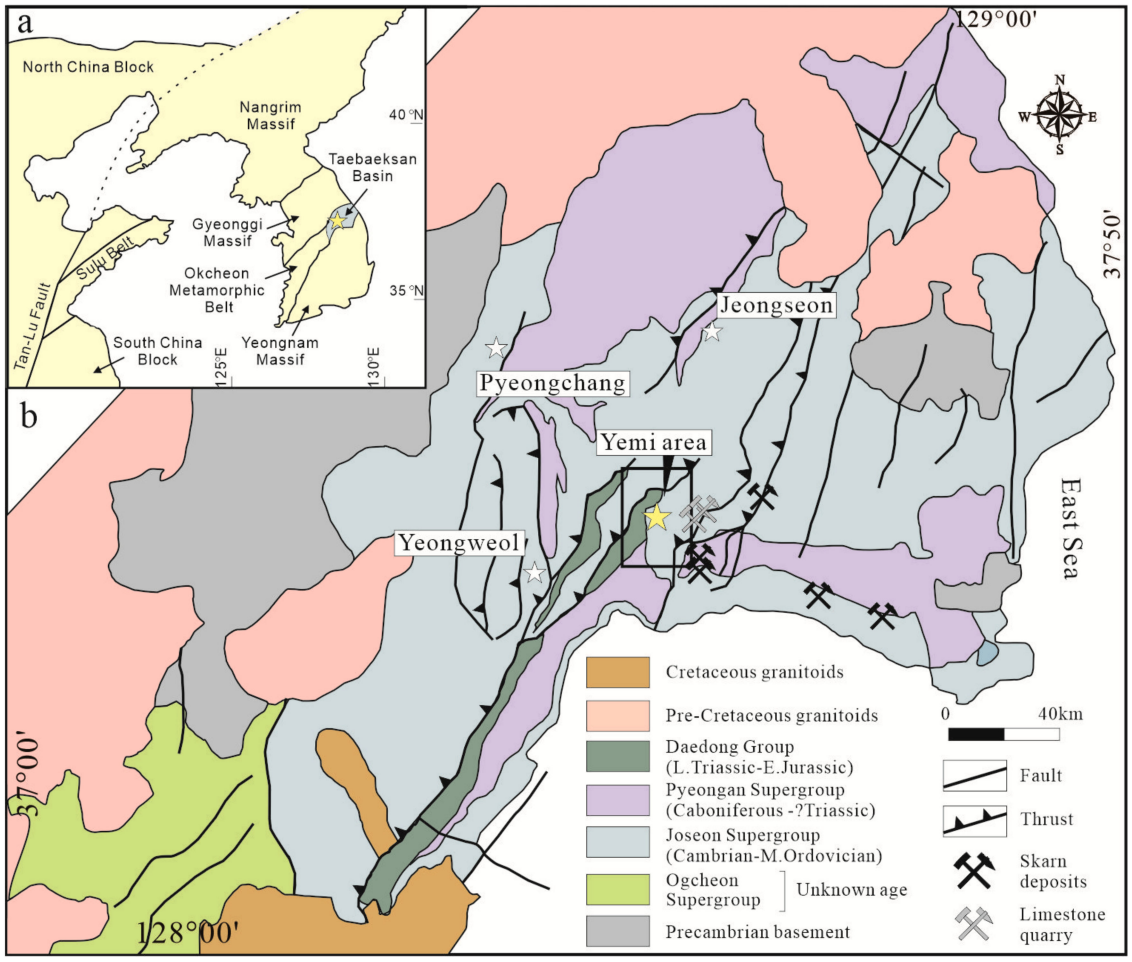

Figure 1. Location of Yemi area and its geological setting. (**a**) Simplified map showing tectonic provinces of East Asia, including the Korean Peninsula, modified from Chough et al. 2000 [19]. (**b**) Geological map showing stratigraphic units of Taebaeksan Basin (modified from [20]). Bold rectangle (Yemi area) shows the study area.

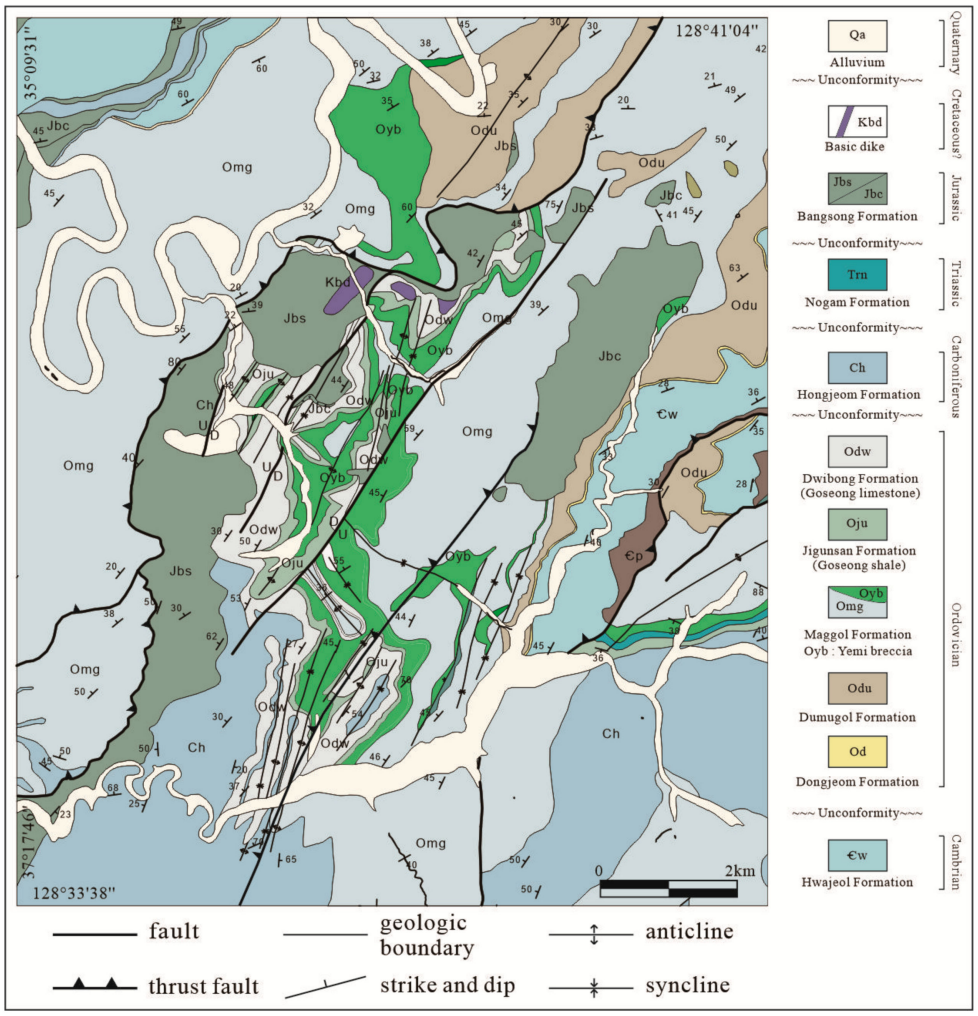

Figure 2. Geologic map of study area modified from Korea Institute of Geoscience and Mineral Resources (KIGAM) (1962) [5,21]. Study area shows tectonic imbrication, formations that are repeated by thrust faults, anticlines, and synclines.

2. Geological Setting

2.1. Regional Geology

Three major Precambrian massifs comprise the Korean Peninsula: the Nangrim, Gyeonggi, and Yeongnam massifs (Figure 1). The Gyeonggi and Yeongnam massifs are separated by the Okcheon Belt, which comprises the weakly metamorphosed Paleozoic Taebaeksan Basin and the Okcheon Metamorphic Belt (OMB). The Taebaeksan Basin includes early Paleozoic marine sedimentary rocks (Joseon Supergroup) and late Paleozoic nonmarine sedimentary rocks (Pyeongan Supergroup), which were folded during the Triassic and Jurassic periods [19]. The Joseon Supergroup is mostly composed of carbonate rock formed mainly in shallow marine and tidal environments, reflecting sea-level changes [19]. The Pyeongsan Supergroup formed mainly in shallow marine, deltaic, and fluvial environments [19]. The Late Triassic to Early Jurassic Daedong Group is composed of conglomerate, sandstone, and shale, which unconformably overlie the Pyeongsan and Joseon Supergroups [22]. Most of the sedimentary rocks in the Taebaeksan Basin are folded, including many well-developed high-angle faults. Cluzel et al. [23,24] insisted that the NS-trending folds and thrust faults were formed by the Songrim Orogeny and the EW-trending folds and faults were developed by the Daebo Event [25]. As a result of these two events, the major geologic structures in the Taebaeksan Basin are commonly NNE- to NE-striking thrusts and associated folds (Figure 1b). Westward-dipping thrust faults dominate in the western part of the basin (Yeongwol area),

while oblique-slip faults and synclines with minor thrusts dominate in the eastern part (Taebaek and Jeongsun areas).

2.2. Local Geology

The Joseon and Pyeongsan Supergroups, and the Bansong Formation mainly comprise the study area. The Joseon Supergroup includes the Hwajeol, Donjeom, Dumugol, Maggol, Jikunsan, and Duwibong Formations, and the Pyeongsan Supergroup contains the Hongjeom, Sadong, Gobangsan, and Nokam Formations (Figure 2). These units have strikes similar to NE-trending thrusts [26]. The Hwajeol Formation is distributed in the southeastern part of the study area and strikes N 30–60° E. The lower part of the Hwajeol Formation is dominated by greenish-gray sandy shale, dark gray sandy slate, greenish-gray slate, dark gray sandy shale, and dark gray fine-grained sandstone, while the upper part shows alternating beds of pinkish-gray limestone and greenish-gray slate [27]. The Dongjeom Formation conformably overlies the Hwajeol Formation. It consists of dark gray and brown medium-grained quartzite and dark brown laminated silicic limestone in the lower part, and dark quartzite in the upper part. This unit strikes N 70–80° W and dips 35–45° NE on average. The Dumugol Formation overlies the Dongjeom quartzite conformably, and consists of greenish-gray slate, greenish-brown slate, brown-green limestone, pinkish-gray limestone, dark gray tabular limestone, and calcareous shale [22]. The Maggol Formation conformably overlies the Dumugol formation and consists of calcic sandstone, dolomite, interbedded calcic conglomerate, and oolitic limestone. It is divided into a lower limestone part and an upper part of alternating dolomite and limestone. The stratigraphic section and the position of the Yemi breccia are reported by Ryu [5].

The carbonate breccia called the Yemi breccia is now known to be a facies of the upper Maggol Formation. It was identified as a separate formation in 1962 [21], but was shown to belong to the upper part of the Maggol Formation by geological, petrological, and paleontological studies [4,5,27]. However, the origin of the Yemi breccia remains controversial. The Jikunsan Formation conformably overlies the Maggol Formation. A shale formation named the Gosung Shale was reported in the study area [21], but Kim (1969) [27] compared it with the Jikunsan Formation based on biostratigraphical data and argued that the two were the same. The formation consists of black shale and bluish-gray limestone, with the lower part dominated by calcareous rocks and the upper part dominated by siliceous rocks [28]. The Dwibong Formation conformably overlies the lower Jikunsan Formation. It is composed of massive pinkish-gray biogenic clastic limestone and calcareous shale [28]. The Hongjeom and Nokam Formations included in the Pyeongsan Supergroup are composed of shale, limestone, and sandstone [29], and are distributed in the southeast of the study area. The Bansong Formation is widely distributed in the study area; its eastern boundary unconformably overlies the Nokam Formation, but the western boundary is truncated by thrust faults. The Bansong Formation is dominated by conglomerate and sandstone with interbedded shale. The linear structures oriented along the NE-SW direction in the study area include bedding, faults, folds, and thrusts, and generally dip to the NW. Several thrust faults developed parallel to the NE-SW direction. These faults are thought to have developed during the Jurassic Daebo Event, after deposition of the Bansong Formation [26].

3. Methods

3.1. Sampling and Carbonate Staining

More than 150 samples were collected during field work for this study. Approximately 60 breccia samples were selected for mineralogical and geochemical studies. Most samples were collected from carbonate units. All collected samples were cut to make slab samples and studied under a stereoscopic microscope. Representative samples were used to make thin sections based on these observations. Thin sections were studied under a petrographic microscope and characterized to determine the genesis of the Yemi breccia, using features such as mineral composition, textures, and mineral relationships.

Samples were stained to distinguish between calcite and dolomite. Alizarin red S stains calcite a red color, while dolomite does not stain; the results depend on the proportion of calcite in the sample and other factors. The Alizarin red S solution was prepared as follows:

$$\underset{\text{(solution)}}{\text{Alizarin red S}} = \underset{\text{(solid)}}{0.1\text{ g Alizarin red S}} + \underset{\text{(liquid)}}{100\text{ g 2\% HCl)}} \quad (1)$$

and, 37% hydrochloric acid was diluted with distilled water to make 2% hydrochloric acid:

$$100\text{ g 2\% HCl} = 5.4\text{ mg 37\% HCl} + 94.6\text{ mg distilled water} \quad (2)$$

All slab samples were stained with Alizarin red S solution in this study. Rocks with irregular surfaces were polished and then stained.

3.2. Electron Probe Microanalysis

Six polished thin sections were selected for electron microprobe analysis to determine their pyrite and hematite geochemistry and gold content. Pyrite and hematite in representative polished thin sections were classified into several types based on morphology, relative minerals, and host rock. The equipment used was a Shimadzu EPMA-1600 electron microprobe analyzer (Shimadzu Corporation, Kyoto, Japan) at Gyeongsang National University to analyze pyrite, hematite, and gold particles. The analysis conditions were acceleration voltage 15 keV, beam current 20 nA, and spot size 1 μm. The elements analyzed were iron, zinc, copper, oxygen, gold, silver, antimony, sulfur, arsenic, cobalt, and lead. Most ore minerals could be identified on backscattered electron (BSE) images, and others required the use of energy-dispersive x-ray spectroscopy (EDS) with the EPMA. In-house standards were used for the analysis the minimum detection limits of the elements are ≤0.01 wt%.

4. Results

4.1. Morphological Features of the Yemi Breccia

The Yemi breccia is widely distributed along a north–south axis near the center of the study area (Figure 2). The Yemi breccia within the Maggol Formation is controlled by bedding planes, and some of it is unrelated to stratigraphy. Most of the breccia observed at the outcrops appears to have poor continuity. Its width, extension, and distribution direction of outcrops vary due to the influence of folds and thrusts. We observed the outcrop of Yemi breccia at 60 points. The Yemi breccia shows three distinct morphologies: crackle, mosaic, and chaotic breccia. This morphological classification, based on textural criteria, generally follows the work of Laznicka (1988) [30]. The Yemi breccia generally occurs as lenticular bodies interbedded with limestone or calcareous silt rocks, showing only one morphological type, although some outcrops show more than one morphology with a gradual transition from one to the other. Figure 3a,b shows a typical crackle breccia, as well as the features that are controlled by the types of host rocks. Field relationships demonstrate that the brecciation developed within the sedimentary layer; calcareous strata are intensively brecciated, while the interbedded silty rocks are not brecciated, and this pattern is common in the study area. Figure 3c shows the features of mosaic and chaotic breccia and a well-preserved sedimentary lamination of the host rock. Some of the breccia has monogenic clasts (Figure 4). Other parts of the breccia, however, have polygenic clasts, including limestone and shale, and dolomitic limestone and shale (Figure 4a,e). These fragments have various shapes, apparently related to the clast mineralogy or the geological environment. Monogenic clast breccias are common throughout the study area. Polygenic clast breccias, however, are generally observed only near the boundary with the overlying Gosung Shale (Jikunsan Formation) (Figure 2).

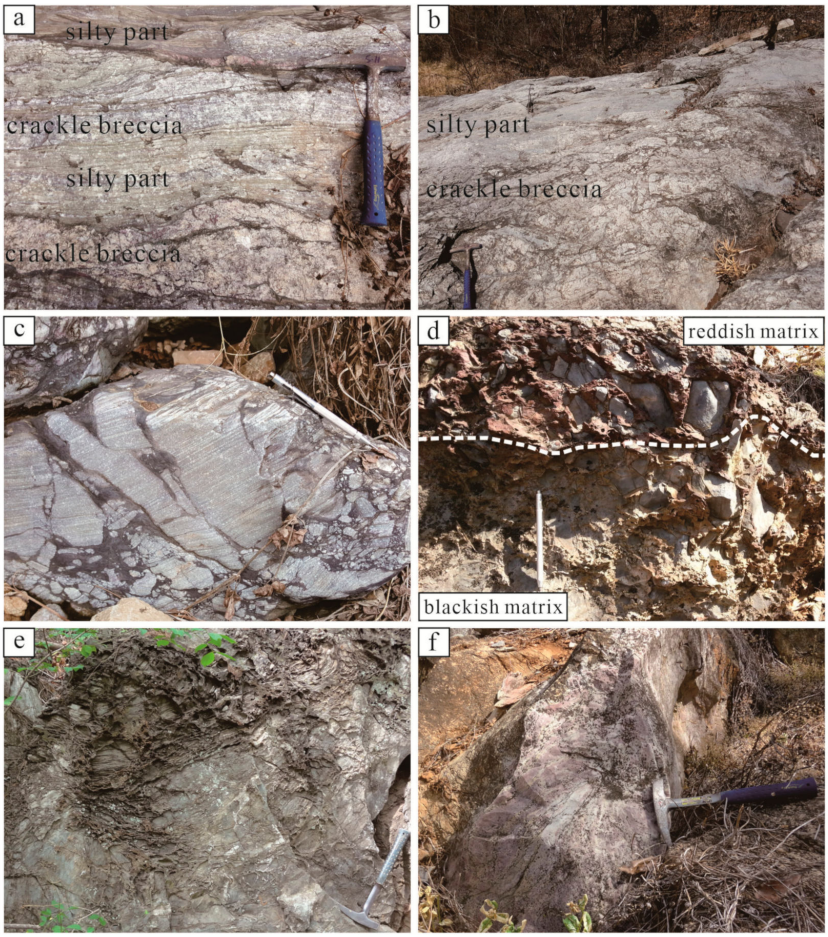

Figure 3. Typical outcrop morphologies of Yemi breccia. (**a**) Stratified breccia with crackle texture. (**b**) Crackle to mosaic texture breccia. (**c**) Mosaic to chaotic texture, with matrix sedimentary layers clearly preserved in fragment. (**d**) Contact of reddish and blackish matrix breccia. Note that the matrix part protrudes more than the clast. It is because of the more weathering-resistant minerals such as hematite in the matrix compared to the more soluble carbonate clasts. (**e**) Mosaic texture breccia with protruding black matrix. (**f**) Mosaic texture breccia composed of white to pinkish materials such as quartz, calcite, and hematite after pyrite.

The Yemi breccia shows various colors because of the matrix materials; it is divided into blackish, reddish, grayish and white to pinkish bodies (Table 1). Blackish matrix breccia (BMB) commonly occurs in bodies that are several meters long (Figure 3e), and their clast size is a few centimeters (1–10 cm; Figure 4a). A commonly observed weathering result is that the matrix protrudes more than the clasts at outcrops (Figure 3d,e). Some parts of blackish matrix breccia change to a yellowish color (Figure 3d). The breccia in Figure 4a has a black matrix and deformed limestone clast, with recrystallized pinkish calcite in the clast. Figure 5a shows the matrix composed of quartz, calcite, pyrite, and an unknown material, presumed to be an insoluble substance or organic material. It has a blackish color because of finely crystalline pyrite and perhaps other unidentified materials. Some parts of the matrix were replaced by quartz (Figure 5e). Quartz, calcite, and pyrite veins are also observed in the BMB (Figure 5f), which developed in Goseong shale. Reddish matrix breccia (RMB) occurs over several meters (3–8 m), and its clast size is a few centimeters (Figure 4d) at the outcrops, similar in occurrence to the BMB. A pattern of differential weathering between the matrix and clasts, comparable to that described above, and is just the result of higher solubility of carbonate minerals in the clasts (Figure 3d,e). RMB generally shows a mosaic texture when observed in the field. Clasts are composed of limestone, dolomite, and shale, and reaction rims are clearly present in limestone fragments (Figure 4b). The RMB matrix mainly

consists of quartz, calcite, minor dolomite, sericite, pyrite, hematite, limonite, and dark unidentified materials, presumed to be insoluble residue or organic material (Figure 5b). In some outcrops, BMB and RMB show a vertical relationship (Figure 3d). In the yellowish part of BMB (Figure 3d), pyrite has been oxidized to goethite or iron oxi-hydroxides (Figure 6), but RMB has hematite (altered pyrite), suggesting that the two breccias formed in different environments. While BMB is dominated by pyrite, RMB is dominated by hematite (Figure 5b). Grayish matrix breccia (GMB) is exposed in outcrops several meters across (Figure 3b), and the outcrops seem to resemble massive or laminated limestone. Boundaries between matrix and clasts are unclear in some samples (Figure 4d). The grayish matrix breccia consists mainly of calcite and dolomite, and minor quartz and pyrite (Figure 5c). GMB also has insoluble residues or organic materials, similar to that observed in BMB and RMB.

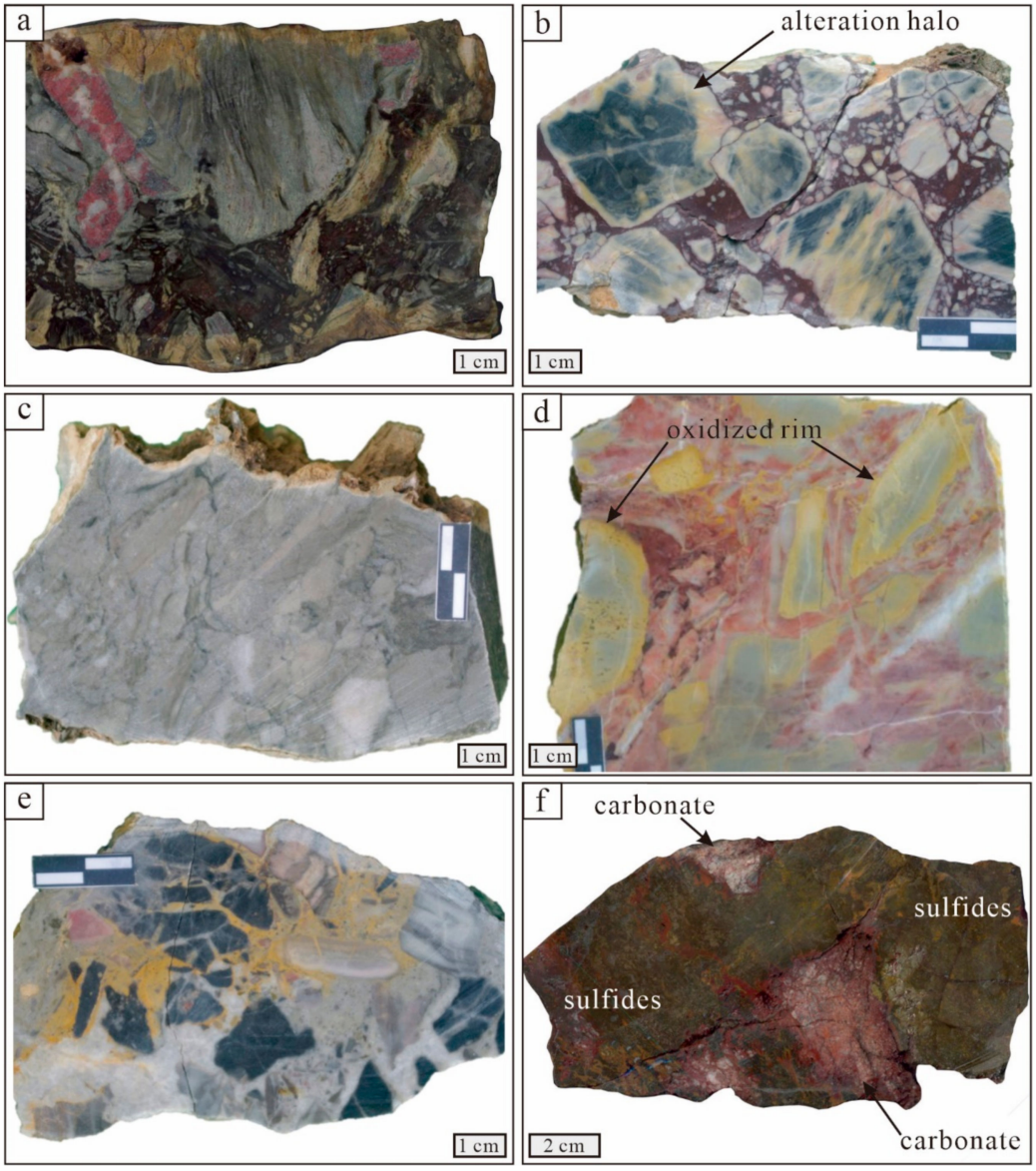

Figure 4. Photographs of slab samples, classified based on matrix materials and colors. (**a**) Polygenic blackish matrix breccia. (**b**) Reddish matrix breccia showing an alteration halo at the clast margin. (**c**) Gray matrix breccia composed of recrystallized calcite and undulating organic materials. (**d**) Pinkish matrix breccia; carbonate clasts have an oxidized rim. (**e**) Gray matrix breccia with angular polygenic clasts. (**f**) Rare sulfide matrix breccia, mostly composed of sulfide minerals such as pyrite, chalcopyrite, and pyrrhotite.

Table 1. Classification of Yemi breccia according to matrix color.

Classes	Minerals	Remarks
Blackish	qz + cal + py + org (+ ep + chl)	Disseminated pyrite, insoluble matter
Reddish	qz + cal + hem (+ org)	Disseminated hematite, alteration halo
Gray	cal + org + py (+ qz)	Disseminated pyrite, crystalline calcite
White to pinkish	cal + py + qz	Crystalline calcite, oxidized rim

Abbreviations: qz, quartz; cal, calcite; py, pyrite; org, organic material; ep, epidote; chl, chlorite; hem, hematite.

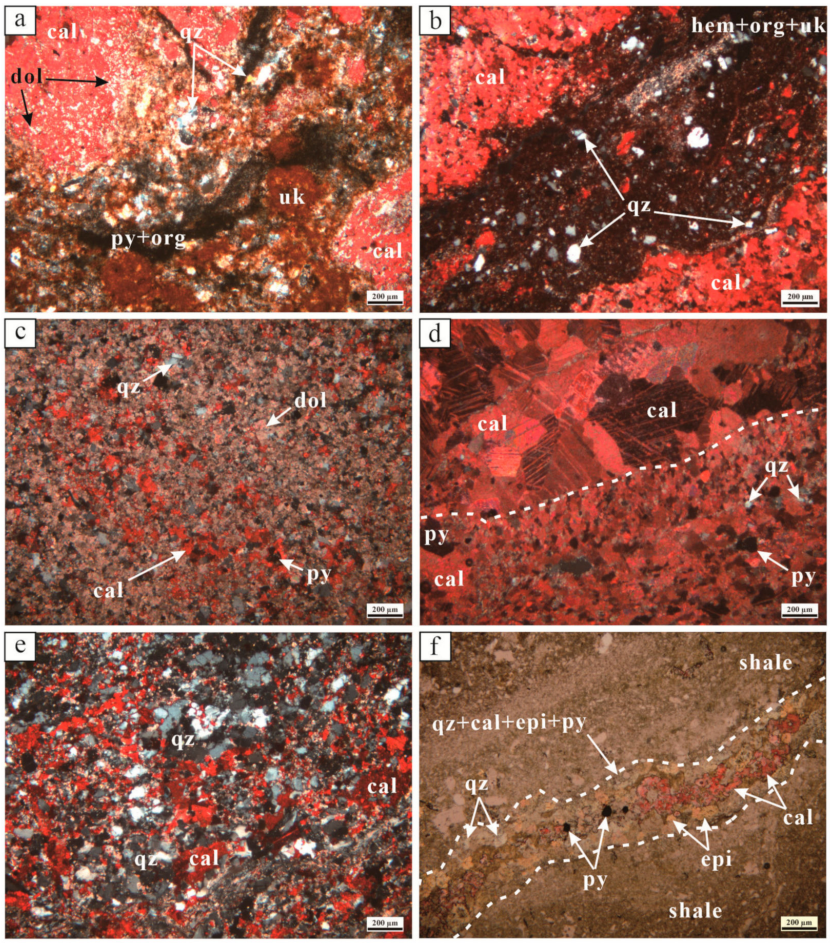

Figure 5. Microphotographs of Yemi breccia. Stained calcite grains have a reddish color. (**a**) Blackish matrix breccia (BMB), composed of quartz, calcite, pyrite, and organic and unknown material. (**b**) Reddish matrix breccia, composed of quartz, calcite, hematite, and organic and unknown material. (**c**) Gray matrix breccia, composed of quartz, calcite, dolomite, and pyrite. (**d**) White to pinkish matrix breccia, composed mainly of calcite replaced by fine-grained quartz, calcite, and pyrite. (**e**) BMB in which calcite is dissolved and replaced by quartz. (**f**) BMB in which quartz + calcite + epidote + pyrite veins occur in shale. Abbreviations: qz, quartz; cal, calcite; dol, dolomite; uk, unknown; py, pyrite; org, organic material; epi, epidote.

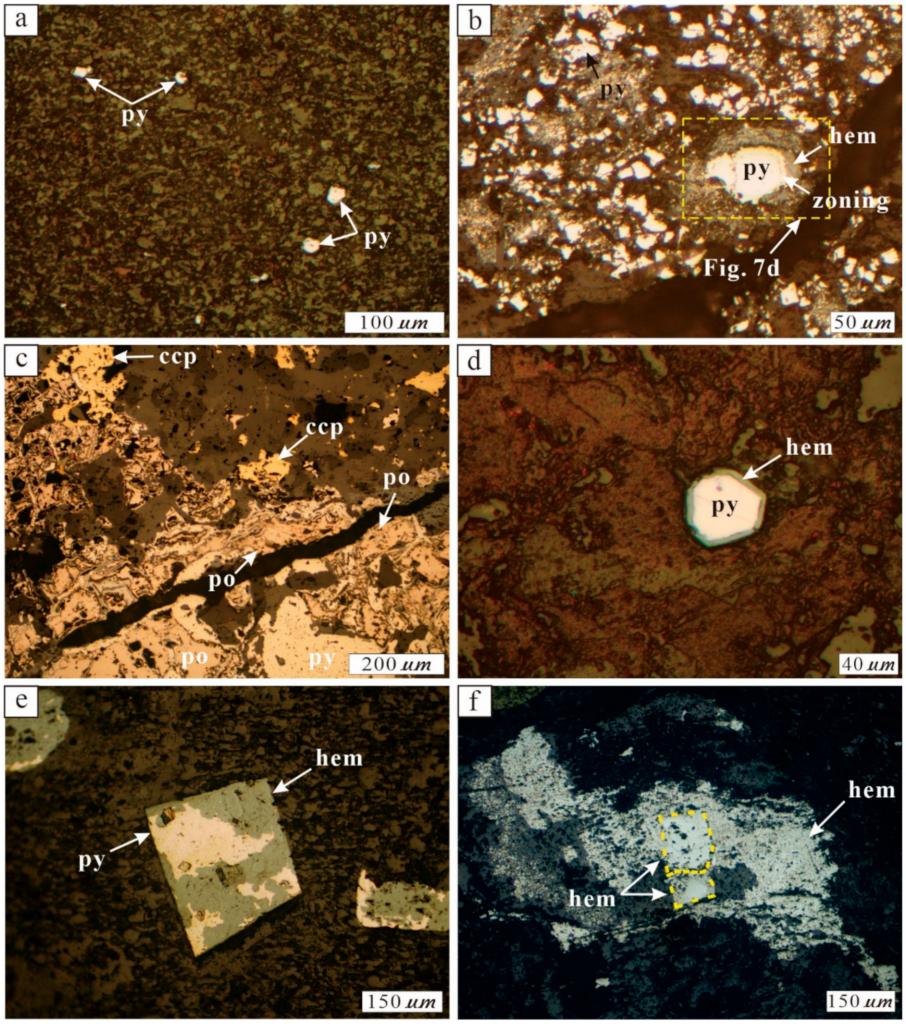

Figure 6. Microphotographs of pyrite and hematite in Yemi breccia. (**a**) Euhedral and disseminated pyrite. (**b**) Irregular pyrite grains. Note overgrowth and replacement textures. (**c**) Pyrite observed with pyrrhotite and chalcopyrite. (**d**) Margin of pyrite altered to hematite. (**e**) Euhedral pyrite partly replaced by hematite. (**f**) Pyrite completely replaced by hematite. Abbreviations: py, pyrite; hem, hematite; ccp, chalcopyrite; po, pyrrhotite.

White to pinkish matrix breccia (WPMB) is common in the study area, and outcrops generally span several meters (Figure 3f). These breccia bodies are noncontiguous and are scattered in the study area. Yellowish clast boundaries indicate oxidation of the disseminated pyrite formed along the clast boundaries (Figure 4d). WPMB is composed of calcite, dolomite, quartz, and pyrite. Coarse-grained calcite is replaced by fine grained quartz, pyrite, and calcite (Figure 5d).

4.2. Occurrence of Metallic Minerals (Mainly Pyrite and Hematite) in Yemi Breccia

The pyrite and hematite in the Yemi breccia show different morphologies and textures (Figure 6 and Table 2). Rare euhedral to subhedral pyrite grains (>20 μm) are disseminated in the carbonate clasts of Yemi breccia (Figure 6a) and may have formed during the diagenesis of carbonate rock. In some parts of the Yemi breccia matrix, euhedral to anhedral pyrite of various size are observed (Figure 6b). Some are coarser (50–200 μm) than others. Coarse-grained pyrite show overgrowth zoning and a change to hematite at the margin of the grain (Figure 6b,d,e and Figure 7d). Some pyrite grains are observed with other sulfides, such as pyrrhotite and chalcopyrite (Figure 6c). Pyrite grains are

replaced by pyrrhotite, and finally precipitated chalcopyrite. Some pyrite was completely changed to hematite (Figure 6f).

Table 2. Characteristics of metallic minerals in Yemi breccia.

	Mineral	Size	Morphology	Remarks
Type 1	Pyrite	<20 μm	Euhedral	Disseminated
Type 2	Pyrite Pyrrhotite Chalcopyrite	20–300 μm >200 μm >200 μm	Euhedral to anhedral, irregular	Disseminated, replacement, overgrowth
Type 3	Hematite	10–200 μm	Euhedral to anhedral, pseudomorph	Disseminated, replacement, overgrowth, overgrowth/replacement

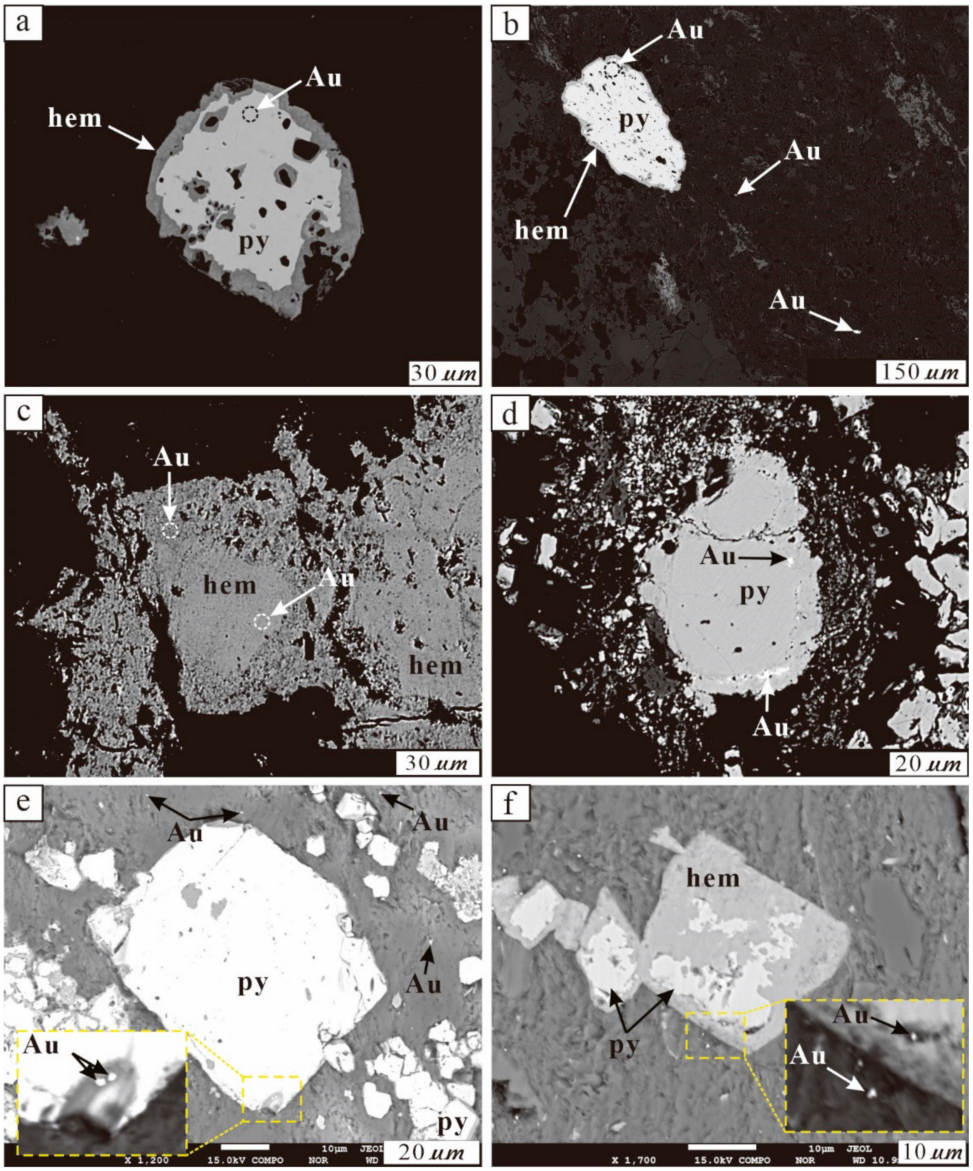

Figure 7. Gold detected within pyrite and hematite. (**a**–**c**) Backscattered electron (BSE) images of pyrite and gold grains from Yemi breccia. (**d**–**f**) Gold particles are observed within pyrite and hematite grains, and isolated at outer parts of pyrite and hematite.

4.3. Occurrence of Gold in Yemi Breccia

In the Yemi breccia, we discovered invisible gold, classified into three types. The first type of gold is invisible under optical and electron microscopes, but confirmed by EPMA analysis of pyrite (Figure 7a,b) and hematite (after pyrite; Figure 7c) grains. The gold content of the pyrite (0.01–1.54 wt%) and hematite (0.07 wt%) ranges from 0.01 to 1.54 wt% (Table 3). These properties are similar to the general characteristics of invisible gold from Carlin-type gold deposits ([31,32] and references therein). The second type of gold is distributed within pyrite and hematite (after pyrite). It is not visible under optical microscopy, but can be confirmed in BSE images from electron microscopy (Figure 7d–f). The particles are irregular, with an average diameter of 0.1 to 5 μm; most of these gold particles are smaller than the beam size (about 1 μm); the gold content is 1.5–12 wt%. Some bright areas in the BSE image are gold particles that occur in zoned pyrite (Figure 7d). The third type of gold is observed at the outer part of pyrite and hematite grains (Figure 7b,e,f). These gold particles range in size from 0.1 to 20 μm. Properties of the second (distributed in pyrite and hematite) and third (isolated grains) types of gold match well with gold from China's Shuiyindong Carlin-type gold deposits [33,34].

Table 3. Result of EPMA (wt%) of the pyrite, hematite, and gold particles

No.	Spot	Fe	Zn	Cu	O	Au	Ag	Sb	S	Co	Pb	Total
1	Pyrite	47.45	<0.01	0.04	3.02	0.68	0.02	<0.01	49.20	0.12	<0.01	100.55
2	Pyrite	45.37	<0.01	0.02	0.45	0.37	0.01	<0.01	53.02	<0.01	<0.01	99.24
3	Pyrite	45.4	<0.01	<0.01	0.26	0.01	<0.01	<0.01	53.3	0.13	0.25	99.32
4	Pyrite	33.1	<0.01	0.06	0.66	0.15	<0.01	0.06	43.9	0.34	14.43	93.08
5	Pyrite	30.89	<0.01	0.04	1.75	1.54	<0.01	<0.01	31.93	<0.01	<0.01	66.61
6	Pyrite	35.67	0.01	0.03	1.61	0.08	0.02	<0.01	36.14	<0.01	<0.01	73.80
7	Pyrite	40.15	<0.01	0.04	2.46	0.03	0.01	<0.01	49.49	<0.01	<0.01	92.37
8	Hematite	68.7	<0.01	<0.01	37.8	0.07	<0.01	<0.01	0.01	0.10	0.09	106.77
9	Au-particle	0.54	<0.01	0.08	25.21	7.00	<0.01	0.06	0.01	0.05	0.01	32.96
10	Au-particle	0.50	<0.01	0.02	23.7	8.64	<0.01	<0.01	0.03	<0.01	0.05	32.92
11	Au-particle	2.05	0.09	0.06	23.41	2.16	<0.01	<0.01	0.41	<0.01	<0.01	28.17

5. Discussion and Conclusions

The Yemi breccia has been studied since it was first discovered in 1962, and many researchers have suggested hypotheses for its genesis. Kim and Kwon (1970) [1] suggested intraformational brecciation or intrusion of argillaceous materials into cracks made by deformation; Reed and Um (1975) [2] suggested synsedimentation breccia-related fault activities; Cluzel (1992) [3] suggested syngenetic fault breccia within an actively forming sediment basin; Woo (1997) [4] suggested solution collapse breccia formed by dissolution; Ryu (2002) [5] suggested debris flow. Based on the differences in genetic mechanisms, carbonate breccia is traditionally summarized into four categories [35]: (1) sedimentary breccia, such as broken debris flow and storm deposition [36–44]; (2) nondepositional breccia, mainly related to karst collapse [45–48]; (3) tectonic breccia, formed by strong tectonic fracturing [49,50]; and (4) diagenetic breccia, formed by pressure dissolution and recrystallization during burial diagenesis [35]. In addition, a nontraditional type of karst, such as hydraulic fracturing [15,16], and hydrothermal karst related to mineralization has been described and summarized [11].

The Yemi breccia, observed at 60 points, can be divided into crackle, mosaic, and chaotic breccias according to the morphology. These breccias are common in karst-collapse and hydraulic fracturing areas [15,16]. The term 'karst' includes underground solution cavities, collapsed breccias, and related topographical features consequent to the dissolution of soluble rocks. Although carbonate dissolution is generally caused by groundwater, it is also caused by hydrothermal fluids; the bodies of rock that result are called 'hydrothermal karst' [6,7,11,51] and show the same morphologies as karst produced by shallow meteoric water. The brecciation which developed within the sedimentary layer demonstrate that calcareous strata are intensively brecciated, while the interbedded silty rocks are not brecciated (Figure 3a,b). It means the insoluble silty strata have not been affected by hydrothermal fluid. The matrix

of the Yemi breccia is composed of mainly quartz, calcite, pyrite, hematite (after pyrite), and insoluble materials showing irregular shape (Table 1). It is different from traditional carbonate breccia and nontraditional hydraulic fractured breccia. Some clasts in the breccia have an alteration halo (Figure 2b). These features are not observed in sedimentary, nondepositional, tectonic, hydraulic fracturing, or diagenetic breccia, but are similar to hydrothermal karst [6,7,52]. The pyrite from the Yemi breccia shows overgrowth and replacement textures (Figure 6). The pyrite that occurred by overgrowth was also replaced by hematite. This means the hydrothermal fluid which precipitated pyrite was introduced more than once. In the Yemi breccia, invisible gold was discovered (Figure 7). This phenomenon is reported in hydrothermal Carlin-type gold deposits [31–34,53,54]. In particular, gold within pyrite and hematite (after pyrite) and isolated gold particles (Figure 7) have been reported in the Shuiyindong deposit [33,34], which is a Carlin-type hydrothermal gold deposit. The evolution model of breccia developed by hydrothermal fluid in limestone and related gold mineralization has been reported [8] in the Carlin-type Conrad zone, Yukon.

In conclusion, the Yemi breccia, developed within the Maggol Formation in the Taebaeksan Basin, has distinct features that can be observed in nontraditional hydrothermal karst. Furthermore, the presence of invisible gold within the breccia is a distinct feature of Carlin-type hydrothermal gold deposits. Thus, we suggest the important role of hydrothermal fluid in karstification within the carbonate Maggol Formation.

Author Contributions: M.-E.P., S.-G.N., B.-C.Y., and S.-H.L. designed and initiated the research. All authors were responsible for mineralogical, petrologic, and geochemical analyses. S.-G.N. prepared the manuscript. All authors have read and agreed to the published version of the manuscript.

Funding: This research was supported by the Basic Research Project of the Korea Institute of Geoscience and Mineral Resources (KIGAM; project no. 20-3211) funded by the Ministry of Science and ICT. This research was also supported by the Basic Research Project of the Korea Institute of Geoscience and Mineral Resources (KIGAM; project no. 15-3211) funded by the Ministry of Science, ICT and Future Planning.

Acknowledgments: We are grateful to anonymous Minerals journal reviewers for their detailed and constructive comments, which led to substantial improvements of the manuscript.

Conflicts of Interest: The authors declare no conflict of interest.

References

1. Kim, O.J.; Kwon, Y.S. Geology of Euirimgil and its vicinity: Special emphasis on the so-called Yemi Limestone Breccia Bed. *J. Geol. Soc. Korea* **1970**, *6*, 213–220.
2. Reed, A.J.; Um, S.H. *The Geology of Korea*; Geological and Mineral Institute of Korea: Seoul, Korea, 1975; p. 139.
3. Cluzel, D. Formation and tectonic evolution of early Mesozoic intramontane basins in the Ogcheon belt (South Korea): A reappraisal of the Jurassic "Daebo orogeny". *J. Southeast Asian Earth Sci.* **1992**, *7*, 223–235. [CrossRef]
4. Woo, K.S. Yemi breccia: The origin and stratigraphic meaning. *Korean J. Pet. Geol.* **1997**, *5*, 16–26.
5. Ryu, I.C. Tectonic and stratigraphic significance of the Middle Ordovician carbonate breccias, Ogcheon Belt, South Korea. *Isl. Asrc* **2002**, *11*, 149–169. [CrossRef]
6. Kunsky, J. Thermomineral karst caves of Zbrashov, northern Moravia. *Sbor. Cs. Spol. Zemepis.* **1957**, *62*, 306–351.
7. Maksimovich, B. *Geologic and Tectonic Relations of Coal-Bearing Senjsko-Resavski Mine and Surrounding Areas*; Jovan, Z., Ed.; Geological Institute: Beograd, Serbia, 1956; p. 104. (In Slovenian)
8. Tucker, M.J.; Hart, C.J.R.; Carne, R.C. Geology, alteration, and mineralization of the Carlin-type Conrad zone, Yukon. In *Yukon Exploration and Geology 2012*; MacFarlane, K.E., Nordling, M.G., Sack, P.J., Eds.; Yukon Geological Survey: Whitehorse, YT, Canada, 2013; pp. 163–178.
9. Smith, M.T.; Rhys, D.; Ross, K.; Lee, C.; Gray, J.N. The Long Canyon Deposit: Anatomy of a New Off-Trend Sedimentary Rock-Hosted Gold Discovery in Northeastern Nevada. *Econ. Geol.* **2013**, *108*, 1119–1145. [CrossRef]

10. Dean, G.; Heitt, W.; Warren, D.; Tommy, B.; Thompson, R.; Jackson, G. Geology and Geochemistry of the Deep Star Gold Deposit, Carlin Trend, Nevada. *Econ. Geol.* **2003**, *98*, 1107–1135. [CrossRef]
11. Andreychouk, V.; Dublyansky, Y.; Ezhov, Y.; Lysenin, G. *Karst in the Earth's Crust: Its Distribution and Principal Types*; University of Silesia and Ukrainian Institute of Speleology and Karstology, Sosnowiec (Poland)-Simferopol (Ukraine): Sosnowiec, Poland, 2009; p. 72.
12. Gustin, M.M.; Smith, M.T. *Technical Report on the Long Canyon Project, Elko County, Nevada, USA: Canadian National Instrument 43-101 Technical Report*; Fronteer Development Group Inc.: Reno, NV, USA, 2009; p. 126.
13. Gustin, M.M.; Smith, M.T.; Simmons, G.L. *Updated Technical Report on the Long Canyon Project, Elko County, Nevada, USA*; Canadian National Instrument 43-101 Technical Report; Fronteer Development Group Inc.: Reno, NV, USA, 2010; p. 137.
14. Williams, C.L. Breccia bodies in the Carlin trend, Elko and Eureka Counties, Nevada: Classification, Interpretation, and Roles in Ore Formation. Master's Thesis, Colorado State University, Fort Collins, CO, USA, 1992; p. 213.
15. Alvarez, W.; Belza, J.; Chan, L.S.; Claeys, P.; Geiser, P.; Menichetti, M.; Shimabukuro, D.H.; Tavarnelli, E. Expansion breccias in Lower Cretaceous Apennine pelagic limestones: I. Geological observations. In *250 Million Years of Earth History in Central Italy: Celebrating 25 Years of the Geological Observatory of Coldigioco: Geological Society of America Special Paper*; Koeberl, C., Bice, D.M., Eds.; The Geological Society of America: Boulder, CO, USA, 2019; Volume 542. [CrossRef]
16. Belza, J.; Alvarez, W.; Tavarnelli, E.; Vanhaecke, F.; Baele, J.-M.; Claeys, P. Expansion breccias in Lower Cretaceous Apennine pelagic limestones: II. Geochemical constraints on their origin. In *250 Million Years of Earth History in Central Italy: Celebrating 25 Years of the Geological Observatory of Coldigioco: Geological Society of America Special Paper*; Koeberl, C., Bice, D.M., Eds.; The Geological Society of America: Boulder, CO, USA, 2019; Volume 542. [CrossRef]
17. Sass-Gustkiewicz, M. Collapse breccia in the ore-bearing dolomite of the Olkusz mine. *Ann. Soc. Geol. Pol.* **1974**, *44*, 217–226.
18. Lubben, J.D. Silicification across the Betze-Post Carlin-Type Au Deposit: Clues to Ore Fluid Properties and Sources, Northern Carlin Trend, Nevada. Ph.D. Thesis, University of Nevada, Las Vegas, NV, USA, 2004.
19. Chough, S.K.; Kwon, S.T.; Ree, J.H.; Choi, D.K. Tectonic and sedimentary evolution of the Korean peninsula: A review and new view. *Earth-Sci. Rev.* **2000**, *52*, 175–235. [CrossRef]
20. Joo, H.; Ryu, I.C. Sedimentary facies of the Cambrian Sesong formation, Taebacksan basin. *J. Econ. Environ. Geol.* **2012**, *45*, 565–578. [CrossRef]
21. Geological Investigation Corps of Taebaegsan Region (GICTR). *Geological Maps of Taebaegsan Region*; Geological Survey of Korea and Geological Society of Korea: Seoul, Korea, 1962.
22. Korea Resources Corporation. *Detailed Reserch Report, DS2001-LS(I)*; Korea Resources Corporation: Wonju-si, Korea, 2001.
23. Cluzel, D.; Cadet, J.P.; Lapierre, H. Geodynamics of the Okcheon belt (South Korea). *Tectonophysics* **1990**, *183*, 41–56. [CrossRef]
24. Cluzel, D.; Jolivet, L.; Cadet, J.P. Early middle Paleozoic intraplate orogeny in the Okcheon belt (South Korea), a new insight on the Paleozoic buildup of east Asia. *Tectonics* **1991**, *10*, 1130–1151. [CrossRef]
25. Kim, J.H.; Lee, J.Y.; Nam, K.H. PreJurassic thrust movement in Danyang area, Danyang coalfield, Korea. *J. Geol. Soc. Korea* **1994**, *30*, 35–40.
26. Kim, J.H.; Lee, J.D. Geologic structures of the Yemi area, Kangweon-do, Korea. *J. Geol. Soc. Korea* **1991**, *27*, 500–514.
27. Kim, B.K. Some new geological aspects revealed from the northwestern part of the Yemi area. *J. Geol. Soc. Korea* **1969**, *5*, 229–241.
28. Min, K.D.; Cho, K.E. Gravity survey of the subsurface geology and geologic structure between Samcheog and Taebaek Area. *Econ. Environ. Geol.* **1995**, *28*, 79–88.
29. The Geological Society of Korea. *Geology of Korea (Seoul, South Korea)*; Sigma Press: Seoul, Korea, 1999; p. 802. (In Korean)
30. Laznicka, P. *Breccias and Coarse Fragmentites: Petrology, Environments, Associations, Ores*; Elsevier: Amsterdam, The Netherlands; New York, NY, USA, 1988; Volume 25, p. 832.

31. Hofstra, A.H.; Cline, J.S. Characteristics and Models for Carlin-Type Gold Deposits. *Rev. Econ. Geol.* **2000**, *13*, 163–220.
32. Large, R.R.; Maslennikov, V.V. Invisible Gold Paragenesis and Geochemistry in Pyrite from Orogenic and Sediment-Hosted Gold Deposits. *Minerals* **2020**, *10*, 339. [CrossRef]
33. Su, W.; Xia, B.; Zhang, H.; Zhang, X.; Hu, R. Visible gold in arsenian pyrite at the Shuiyindong Carlin-type gold deposit, Guizhou, China: Implications for the environment and processes of ore formation. *Ore Geol. Rev.* **2008**, *33*, 667–679. [CrossRef]
34. Su, W.; Zhang, H.; Hu, R.; Ge, X.; Xia, B.; Chen, Y.; Zhu, C. Mineralogy and geochemistry of gold-bearing arsenian pyrite from the Shuiyindong Carlin-type gold deposit, Guizhou, China: Implications for gold depositional processes. *Miner. Depos.* **2012**, *47*, 653–662. [CrossRef]
35. Flügel, E. *Microfacies of Carbonate Rocks: Analysis, Interpretation and Application*; Springer: Berlin, Germany, 2004.
36. Ryu, I.C.; Doh, S.J.; Choi, S.G. Carbonate breccias in the lower-middle Ordovician Maggol limestone (Taebaeksan Basin, South Korea): Implications for regional tectonism. *Facies* **2002**, *46*, 35–56. [CrossRef]
37. Frédéric, B.; Michel, S.; Alexis, M. Coarse carbonate breccias as a result of water-wave cyclic loading (uppermost Jurassic–South-East Basin, France). *Sedimentology* **2001**, *48*, 767–789.
38. Seguret, M.; Moussine-Pouchkine, A.; Gabaglia, G.R.; Bouchette, F. Storm deposits and storm-generated coarse carbonate breccias on a pelagic outer shelf (South-East Basin, France). *Sedimentology* **2001**, *48*, 231–254. [CrossRef]
39. Payros, A.; Pujalte, V.; Orue-Etxebarria, X. The South Pyrenean Eocene carbonate megabreccias revisited: New interpretation based on evidence from the Pamplona Basin. *Sediment. Geol.* **1999**, *125*, 165–194. [CrossRef]
40. Hong, Q. The carbonate gravity flow sediments in the juncture of Yunnan, Guizhou and Guangxi. *J. Southwest Pet. Inst.* **1982**, *4*, 1–11.
41. Mei, Z.; Chen, J.; Lu, H.; Li, H. Deep water carbonate debris flow in the middle Ordovician Pingliang formation of Fuping, Shaanxi. *Oil Gas Geol.* **1982**, *3*, 49–56.
42. Carbonate Rock Research Office. Deep water carbonate brecclas in the Nanpan river area during the Permian and Triassic periods. *J. Southwest Pet. Inst.* **1982**, *4*, 1–26.
43. Luo, Z. Preliminary study on Triassic and late Paleoxoic reef facies in Yunnan-Guizhou-Guangxi region and their Petroleum prospect. *Exp. Pet. Geol.* **1983**, *5*, 18–28.
44. Du, Y.; Li, S.; Jia, Z.; Wang, S. Re-discussion on the origin of the rudstone in Middle Permian Qixia Formation along Lower Yangtze River of Anhui Province. *Geol. Rev.* **2012**, *58*, 426–433.
45. Blount, D.N.; Moore, C.H. Depositional and non-depositional carbonate breccias, Chiantla Quadrangle, Guatemala. *Geol. Soc. Am. Bull.* **1969**, *80*, 429–442. [CrossRef]
46. Morrow, D.W. Descriptive field classification of sedimentary and diagenetic breccia fabrics in carbonate rocks. *Bull. Can. Pet. Geol.* **1982**, *30*, 227–229.
47. Liu, H.; Ma, T.; Tan, X.; Zeng, W.; Hu, G.; Xiao, D.; Luo, B.; Shan, S.; Su, C. Origin of structurally controlled hydrothermal dolomite in epigenetic karst system during shallow burial: An example from Middle Permian Maokou Formation, central Sichuan Basin, SW China. *Pet. Explor. Dev.* **2016**, *43*, 1000–1012. [CrossRef]
48. Li, W.; Zhang, Y.; Zhang, B.; Li, J.; Wang, J.; Ma, X. Origin, characteristics and significance of collapsed-paleocave systems in Sinian to Permian carbonate strata in Central Sichuan Basin, SW China. *Pet. Explor. Dev.* **2014**, *41*, 513–522. [CrossRef]
49. Wilshire, H.G.; Howard, K.A.; Offield, T.W. Impact breccias in carbonate rocks, Sierra Madera, Texas. *Geol. Soc. Am. Bull.* **1971**, *82*, 1009–1017. [CrossRef]
50. Tarasewicz, J.P.T.; Woodcock, N.H.; Dickson, J.A.D. Carbonate dilation breccias: Examples from the damage zone to the Dent Fault, northwest England. *Geol. Soc. Am. Bull.* **2005**, *117*, 6722–6723. [CrossRef]
51. Kutyrev, E.I.; Michailov, B.M.; Liakhnitsky, Y.S. *Karstovye 68 Mestorozdenia (Karstic Mineral Deposits)*; Nedra: Leningrad, Russia, 1989; p. 311. (In Russian)
52. Dristas, J.A.; Martinez, J.C.; Kerkhof, A.M.; Massonne, H.J.; Theye, T.; Frisicale, M.C.; Gregori, D.A. Hydrothermal karst and associated breccias in Neoproterozoic limestone from the Barker-Villa Cacique area (Tandilia belt), Argentina. *J. S. Am. Earth Sci.* **2017**, *76*, 182–197. [CrossRef]

53. Reich, M.; Kesler, S.E.; Utsunoyiya, S.; Palenik, C.S.; Chryssoulis, S.; Ewing, R.C. Solubility of gold in arsenian pyrite. *Geochim. Cosmochim. Acta* **2005**, *69*, 2781–2796. [CrossRef]
54. Arehart, G.B.; Eldridge, C.S.; Chryssoulis, S.L.; Kesler, S.E. Ion microprobe determination of sulfur isotope variations in iron sulfides from the Post/Betze sediment-hosted disseminated gold deposit, Nevada, USA. *Geochim. Cosmochim. Acta* **1993**, *57*, 1505–1519. [CrossRef]